scientific reports

Check for updates

OPEN

Alteration in Golgi apparatus fragmentation related genes in human dilated cardiomyopathy

Irene González-Torrent[1,3], Isaac Giménez-Escamilla[1,2,3], Lorena Pérez-Carrillo[1,2], Marta Delgado-Arija[1,2], Manuel Portolés[1,2], Estefanía Tarazón[1,2,3]✉ & Esther Roselló-Lletí[1,2,3]✉

The Golgi apparatus (GA) plays a main role in the protein secretory pathway. Previously, we described a greater GA vesicle density in patients with dilated cardiomyopathy (DCM), as well as an increase in natriuretic peptide (NP) levels inside these vesicles. GA fragmentation could increase the rate of protein transport; for this reason, we aimed to delve deeper into these GA vesicle density alterations by studying the expression of genes related to GA architecture in DCM and its relationship with NP levels. We performed RNA-seq analysis on explanted hearts from DCM patients ($n = 13$) and control (CNT) individuals ($n = 10$). We detected alterations in molecules related to the structure and positioning of GA, highlighting the decrease in GM130 levels and increase in the p-GM130/GM130 ratio ($p < 0.05$) observed via Western blotting (DCM, $n = 23$; CNT, $n = 7$) and their correlation with NT-proBNP levels ($r = -0.473$, $p < 0.05$; $r = 0.455$, $p < 0.05$; respectively). We also observed an upregulation of genes involved in anterograde transport and a downregulation of genes involved in retrograde transport. Moreover, we visualized GA fragmentation in doxorubicin-induced DCM in AC16 cells via immunofluorescence (70.2% of the cells had fragmented GA, $p < 0.05$) and corroborated the downregulation of *GOLGA2* and the increase in NP levels observed in human tissue. Our results revealed dysregulation of genes that maintain GA structure, suggesting that GA fragmentation occurs in DCM patients. Therefore, the imbalance between anterograde and retrograde transport could also contribute to this situation and to increased formation of transport vesicles.

Keywords Dilated cardiomyopathy, Golgi fragmentation, Vesicle transport, GM130, Natriuretic peptides

Dilated cardiomyopathy (DCM), one of the most common causes of heart failure (HF)[1], is characterized by left ventricular or biventricular dilation and impaired contraction that is not explained by abnormal loading conditions (for example, hypertension and valvular heart disease) or coronary artery disease[2]. The impaired myocardial function has been attributed in part to alterations in the function of contractile proteins and excitation–contraction coupling (ECC)[3]. This disease has been associated with several cellular alterations in cardiac tissue, such as mitochondrial dysfunction[4] and endoplasmic reticulum stress[5]. However, the role of the Golgi apparatus (GA) in this disease has been less studied.

The GA is the central organelle of the secretory pathway responsible for processing and packaging proteins. It consists of polarized stacks of flattened cisternae connected by tubular bridges; localized at the perinuclear region. This architecture is maintained by Golgi matrix proteins, proteins of the transport machinery, and the cytoskeleton and their associated proteins[6]. The GA is not a static organelle; the loss of the Golgi ribbon and the dispersion of fragmented GA throughout the cytoplasm occur during many physiological processes, such as mitosis and apoptosis[7]. Furthermore, these perturbations have also been associated with diseases, such as Alzheimer's disease[8] and cancer[9]. GA alteration may impair accurate modification, trafficking, and sorting of proteins[8]. Several molecules are related to GA fragmentation, especially GM130, a golgin located in the cis-Golgi. Its deletion leads to disrupted organization[10], as does its phosphorylation at Ser25[11].

In previous studies[12], we reported that morphological alterations in Golgi vesicles in patients with DCM are linked to worsening function. Compared with controls (CNT), patients with DCM had more numerous,

[1]Clinical and Translational Research in Cardiology Unit, Health Research Institute Hospital La Fe (IIS La Fe), Avd. Fernando Abril Martorell, 106, 46026 Valencia, Spain. [2]Center for Biomedical Research Network on Cardiovascular Diseases (CIBERCV), Avd. Monforte de Lemos 3-5, 28029 Madrid, Spain. [3]Irene González Torrent, Isaac Giménez Escamilla, Estefanía Tarazón and Esther Roselló Lletí contributed equally to this work. ✉email: estefania_tarazon@iislafe.es; esther_rosello@iislafe.es

smaller, and ellipsoidal vesicles with a higher natriuretic peptide (NP) concentration, indicating that GA plays an important role in the response to increasing NP demand in DCM. NPs are released to protect against the effects of pressure and volume overload. Among them, B-type natriuretic peptide (BNP) and N-terminal proBNP (NT-proBNP) are widely used as diagnostic and prognostic biomarkers of HF[13].

Considering the abovementioned findings, we hypothesized that GA fragmentation may be related to the morphological vesicular alteration we previously observed in DCM in response to an increase in NP demand. To explore the state of GA in DCM patients, we focused our investigation on the expression and phosphorylation of GM130, as one of the main molecules related to GA fragmentation, and its relationship with NP levels. We also further studied the expression of other genes involved in GA structure, cytoskeleton and vesicle transport that may be involved with the disruption of this organelle. Finally, we used a doxorubicin-induced DCM in vitro model to confirm our findings.

Methods

Tissue sample collection

Myocardial tissue samples were obtained from near the apex of the left ventricle of patients with DCM who were undergoing cardiac transplantation. After extraction, the samples were maintained in 0.9% NaCl at 4 °C for a maximum of 4.4 ± 3 h after the loss of coronary circulation and stored at − 80 °C until use.

All available data were collected for each patient: clinical history, electrocardiograms, Doppler echocardiography, hemodynamic studies, and coronary angiography (Table 1). DCM was diagnosed when patients had LV systolic dysfunction (ejection fraction (EF) < 40%) with a dilated left ventricle (LV end-diastolic diameter (LVEDD) > 55 mm) on echocardiography. None of the patients had existing primary valvular disease. All patients were functionally classified according to the functional criteria of the New York Heart Association (NYHA) and received medical treatment according to the guidelines of the European Society of Cardiology[13]. CNT samples were obtained from nondiseased hearts that were rejected for heart transplantation due to size or blood incompatibility. The causes of death of the donors were cerebrovascular events or motor vehicle accidents. CNT hearts had normal LV function (EF > 50%) and no history of prior heart disease. Only age and sex data were available in accordance with the Spanish Organic Law on Data Protection 15/1999. This investigation was approved by the Ethics Committee (Biomedical Investigation Ethics Committee of La Fe University Hospital of Valencia, Spain) and was conducted in accordance with the principles outlined in the Declaration of Helsinki[14]. Prior to tissue collection, signed informed consent was obtained from each patient.

RNA extraction and sequencing

Heart samples (DCM, $n = 13$; CNT, $n = 10$) were homogenized with TRIzol agent in a TissueLyser LT (Qiagen, UK). The RNA isolation and RNA-seq procedures and analyses have been extensively described previously by Roselló-Lletí et al.[15]. Briefly, RNA was extracted using the PureLink™ Kit (Ambion Life Technologies, USA), and cDNA libraries were obtained following Illumina's recommendations. Sequencing was performed through SOLiD 5500xl platform.

	RNA-seq analysis ($n = 13$)	Protein analysis ($n = 23$)
Male sex (%)	92	74
Age (years)	51 ± 11	50 ± 14
NYHA class	III-IV	III-IV
Prior hypertension (%)	17	20
Prior smoking (%)	50	53
Diabetes mellitus (%)	17	19
BMI (kg/m^2)	27 ± 5	25 ± 5
Haemoglobin (g/dL)	13 ± 3	13 ± 3
Haematocrit (%)	39 ± 7	39 ± 6
Total cholesterol (mg/dL)	147 ± 37	133 ± 38
LVEF (%)	17 ± 8	20 ± 9
LVESD (mm)	74 ± 10	66 ± 12
LVEDD (mm)	82 ± 8	74 ± 11
Controlcharacteristics	$n = 10$	$n = 7$
Gender male (%)	80	57
Age (years)	47 ± 16	57 ± 21
LVEF (%)	> 50	> 50

Table 1. Clinical characteristics of patients with dilated cardiomyopathy and controls. Qualitative data are presented as percentages, and quantitative data are presented as the means ± standard deviations. NYHA, New York heart association; BMI, body mass index; LVEF, left ventricle ejection fraction; LVESD, left ventricular end-systolic diameter; LVEDD, left ventricular end-diastolic diameter.

Homogenization of samples and protein determination

Protein extraction and determination from the LV samples (DCM, $n=23$; CNT, $n=7$) have been extensively described previously by Roselló-Lletí et al.[15]. Briefly, 25 mg of the LV samples were homogenized with the FastPrep-24 homogenizer (MP Biomedicals, USA) in extraction buffer (2% SDS, 10 mM EDTA, and 6 mM Tris–HCl, pH 7.4) with protease inhibitors (25 µg/ml aprotinin and 10 µg/ml leupeptin). The homogenates were centrifuged, and the supernatant was aliquoted. The protein content was determined via Peterson's modification[16] of the micro-Lowry method with bovine serum albumin (BSA) as the standard.

Polyacrylamide gel electrophoresis and Western blot analysis

Protein samples for the detection of NT-proBNP, CDK5, GM130 and GM130 phosphorylated at Ser25 (p-GM130) were separated via Bis-Tris Midi gel electrophoresis with 4–12% polyacrylamide. After electrophoresis, the proteins were transferred from the gel to a PVDF membrane via the iBlot Dry Blotting System (Invitrogen, UK) for Western blot analyses. The membranes were blocked overnight at 4 °C with 1% BSA in Tris-buffer solution containing 0.05% Tween 20, after which they were incubated for 2 h with the primary antibody in the same buffer. The primary detection antibodies used were as follows: anti-NT-proBNP (1:300 dilution, 4NT1, HyTest, Finland), anti-CDK5 rabbit monoclonal antibody (1:500 dilution, ab40773, Abcam, UK), anti-GM130 rabbit monoclonal antibody (1:500 dilution, ab52649, Abcam, UK), and anti-p-GM130 mouse monoclonal antibody directed against GM130 phosphorylated at serine 25 (1:100 dilution, sc-377549, Santa Cruz Biotechnology, USA). A mouse monoclonal antibody against GAPDH (1:1000 dilution, ab8245, Abcam, UK) was used as the loading control.

The bands were visualized via an acid phosphatase-conjugated secondary antibody and a nitro blue tetrazolium/5-bromo-4-chloro-3-indolyl phosphate (NBT/BCIP, Sigma-Aldrich, USA) substrate system. Finally, the bands were digitalized via an image analyzer (DNR Bio-Imagining Systems, Israel) and quantified via the GelQuant Pro (v.12.2) program.

Cell culture

The AC16 human cardiomyocytes cell line (SCC109, Merck, USA) was cultured in DMEM/F12 medium (11330-032, Gibco, UK) supplemented with 12.5% fetal bovine serum, 2 mM L-glutamine and 1X penicillin–streptomycin solution at 37 °C in a 5% CO_2 incubator. The cells were seeded at 1×10^5 cells/well on cover glasses and treated with 12.5 mg/ml fibronectin (F1141, Sigma Aldrich, USA) and 200 mg/ml gelatin (G1393, Sigma Aldrich, USA) in 24-well plates. After reaching 80% confluence, the cells were treated with doxorubicin (DOX) (HY-15142, MedChem Express, USA) at a concentration of 450 nM for 48 h toinduce DCM.

Immunofluorescence

AC16 cells were fixed in PBS containing 4% paraformaldehyde for 20 min at room temperature and treated with NH4Cl to block aldehyde groups. For permeabilization, the cells were incubated with PBS containing 10% FBS, 1% BSA and 0.1% Triton X-100 for 15 min. Coverslips were incubated with an anti-GM130 primary antibody (1:200 dilution, ab52649, Abcam, UK) overnight and then with an Alexa Fluor 488-conjugated secondary antibody (1:50 dilution, ab150077, Abcam, UK) for 30 min. Finally, the coverslips were mounted in Vectashield with DAPI (H-1200-10, Vector Laboratories, USA) to visualize the nuclei. Three independent experiments were performed. Images were acquired with a Nikon Eclipse Ts2R microscope (Nikon Instruments Inc., Netherlands) with a 60X objective for Golgi fragment quantification and 40X and 100X oil immersion objectives for the images shown. Golgi fragments and the nucleus area were quantified in at least 150 cells per experiment via the Analyze Particle plugin in ImageJ software (v.1.53e; National Institutes of Health, USA). Previously, background subtraction was performed, and a threshold was fixed. The criterion to consider that cells had GA fragmentation was having more than 15 Golgi fragments that were less than 1 μm^2, as established by Nozawa et al.[17].

Reverse transcription and quantitative PCR

Total RNA was isolated from AC16 cells treated with DOX ($n=4$) or left untreated ($n=5$) via the miRNeasy Mini Kit (217004, Qiagen, Germany) following the instructions provided by the manufacturer. The RNA was eluted in 30 µL of RNase-free water. Complementary DNA synthesis was performed with 100 µg of total RNA using the reverse transcriptase M-MLV (28025013, Invitrogen, USA) following the manufacturer's protocol. The reverse transcription reaction product was used for quantitative PCR (qPCR) performed via the TaqMan Gene Expression Assay in a QuantStudio 5 Real-Time PCR System (A34322, Applied Biosystems, USA) according to the manufacturer's instructions. The following TaqMan probes were obtained from Applied Biosystems: *GOLGA2* (Hs00366395_m1), and *NPPB* (Hs00173590_m1). *GAPDH* was used as an endogenous reference (Hs99999905_m1). The $2^{-\Delta\Delta Ct}$ method was used to compare relative expression between samples from the different groups[18].

ELISA

BNP protein levels were measured in 12 cell culture supernatant samples from DOX-treated cells ($n=6$) and untreated cells ($n=6$). BNP levels were assessed via specific sandwich enzyme-linked immunosorbent assays with a Human BNP Elisa Kit (ab193694, Abcam, UK) according to the manufacturer´s instructions. The BNP test has a limit of detection of 14 pg/ml. The test was quantified at 450 nm in a dual-wavelength microplate reader (Sunrise, Tecan, Switzerland) via Magellan version 2.5 software (Tecan, Switzerland).

Identification of protein–protein interactions

A Protein–protein interactions network was constructed via the STRING database v12 (available at https://string-db.org/). The interaction sources included experiments, databases, and coexpression analyses. A medium level of confidence (0.4) was chosen. The molecules were classified according to different GO terms: component

of the Golgi membrane (GO:0000139), protein involved in vesicle-mediated transport (GO:0016192) and its regulation (GO:0060627), and structural constituent of the cytoskeleton (GO:0005200).

Statistical analysis

Clinical characteristics are expressed as the means ± standard deviations (SDs) for continuous variables and as percentage values for discrete variables. The distribution of the variables was analyzed via the Kolmogorov–Smirnov test. The clinical characteristics of patients were compared via Student's t test for continuous variables and Fisher's exact test for discrete variables. Differential RNA expression analysis between conditions was performed via the DESeq2 method (version 3.4, available at http://www.bioconductor.org/packages/release/bioc/html/DESeq2.html)[19]. We considered those RNAs with a p value corrected by FDR (P adj) ≤ 0.05 as differentially expressed to avoid the identification of false positives across the differential expression data[20]. Gene predictions were estimated using the Cufflinks method[21], and the expression levels were calculated via HTSeq software (version 0.5.4p323, available at https://pypi.python.org/pypi/HTSeq)[22]. This method eliminates the multimapped reads, and only the unique reads are considered for gene expression estimation. The edgeR method (version 3.2.4, available at https://bioconductor.org/packages/3.20/bioc/html/edgeR.html) was applied for differential expression analysis between conditions[23]. This method relies on different normalization processes based on in-depth global samples, CG compositions and lengths of genes. In the differential expression process, this method relies on a Poisson model to estimate the variance of the RNA-seq data for differential expression. Significant mean differences in molecule levels were analyzed via Student's t test for variables with a normal distribution and the Mann–Whitney U test for variables with a nonnormal distribution. Finally, Pearson's correlation coefficients were calculated to determine the relationships among variables with a normal distribution. $p < 0.05$ was considered statistically significant. All statistical analyses were performed via SPSS (v.20.0) software (IBM SPSS Inc., USA), R (version R-4.3.1) or GraphPad Prism 8.

Results

Clinical characteristics of patients

The patients' clinical and echocardiographic characteristics are summarized in Table 1. The patients with DCM were mostly men (72%), with a mean age of 51 ± 14 years, and they were classified as classes III–IV according to the NYHA functional classification. In addition, they had been previously diagnosed with different comorbidities, such as hypertension (18%) and diabetes mellitus (17%). The CNT group also consisted mainly of men (71%), with a mean age of 53 ± 17 years (Table 1). Comorbidities and other echocardiographic data were not available for the CNT group, in accordance with the Spanish Organic Law on Data Protection 15/1999.

GA organization and vesicle transport analysis in patients with DCM

To investigate transcriptome-level differences between CNT ($n = 10$) and DCM ($n = 13$) samples, a large-scale screening study was performed using RNA-seq technology. We analyzed 183 genes related to GA structure and positioning and vesicle transport (Supplementary Table S1), 23 of which were differentially expressed ($p < 0.05$) (Fig. 1A). Through the STRING database, we performed a protein–protein interaction network analysis of the genes found to be altered in DCM, and we classified them according to different GO terms (Fig. 1B). In this figure, we also present correlations that we found in DCM patients between the mRNA expression of genes whose expression was altered (Table 2).

GA structure and positioning-related genes in patients with DCM

We focused on the expression of *GOLGA2*, which encodes golgin GM130, due to its role in GA fragmentation. We found that this gene was downregulated (FC = − 1.23, $p < 0.01$) in patients with DCM compared CNT subjects (Fig. 2A). Next, we measured the GM130 and p-GM130 protein levels via Western blot analysis. We observed a significant decrease in GM130 levels (FC = − 1.37, $p < 0.05$) and an increase in the p-GM130/GM130 ratio (FC = 1.25, $p < 0.05$) in patients with DCM patients (Fig. 2B and C, respectively). Furthermore, we determined whether there was any relationship between this protein and NPs, and interestingly, we observed that NT-proBNP was inversely related to GM130 levels ($r = -0.473$, $p < 0.05$) and directly related to the ratio of GM130 phosphorylation ($r = 0.442$, $p < 0.05$) (Fig. 2D and E, respectively). GM130 is a substrate of the kinase CDK5[11], and accordingly, we detected an upregulation of *CDK5* (FC = 1.49, $p < 0.05$) in DCM (Fig. 2F).

We analyzed the mRNA levels of other Golgi matrix proteins that maintain the ribbon structure of GA and found that golgin *TMF1* expression was lower in the DCM group than in the CNT group (FC = − 1.22, $p < 0.05$) (Fig. 2G). Several of these structural proteins can be cleaved by caspases;[4] therefore, we analyzed them and found that *CASP2* was upregulated (FC = 1.29, $p < 0.05$) (Fig. 2H).

GA structure and positioning also depend on the cytoskeleton, so we analyzed tubulin and the actin family. We observed that an actin subunit, *ACTA1*, was upregulated (FC = 2.66, $p < 0.001$) (Fig. 2I), and three subunits of the microtubules were altered: *TUBA3E* (FC = − 2.15, $p < 0.01$), *TUBA1A* (FC = 1.91, $p < 0.001$), and *TUBA4A* (FC = 1.81, $p < 0.01$) (Fig. 2J). Finally, we examined associated molecules involved in the interaction of GA with the cytoskeleton and found that *CLIP3* was upregulated (FC = 1.41, $p < 0.001$) in patients with DCM (Fig. 2K).

Vesicle transport-related genes in patients with DCM

We examined the genes involved in vesicle transport. Specifically, in the anterograde transport, we detected decreased expression of *AP1S2* (FC = − 1.38, $p < 0.05$) and increased expression of several genes: *AP1M1* (FC = 1.27, $p < 0.01$), *VPS41* (FC = 1.26, $p < 0.05$), *LMAN2L* (FC = 1.58, $p < 0.001$), *KIF13A* (FC = 1.37, $p < 0.01$), *SEC31A* (FC = 1.20, $p < 0.01$), *SORT1* (FC = 1.64, $p < 0.001$), and *TRAPPC2* (FC = 1.56, $p < 0.01$) (Fig. 3A); when we compared patients with DCM with those in the CNT group. Moreover, in retrograde transport, three members of the Rab family, *RAB9A* (FC = − 1.64, $p < 0.01$), *RAB9B* (FC = − 1.40, $p < 0.05$) and *RAB29*

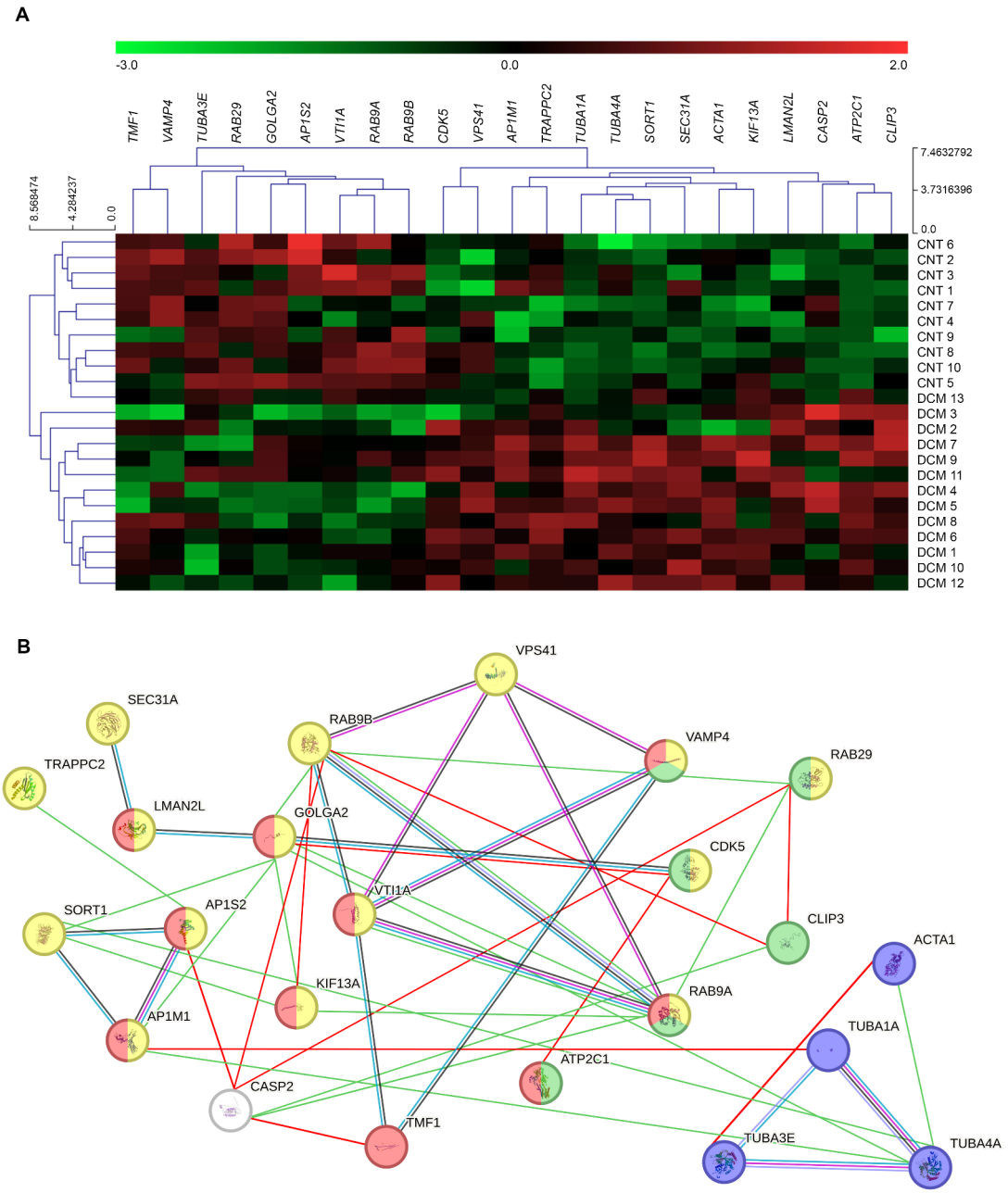

GO-term	Description	Count in network	Strength	FDR	Colour
GO:0000139	Golgi membrane	10 of 664	1.11	2.90e-07	
GO:0016192	Vesicle-mediated transport	15 of 1298	0.97	0.0289	
GO:0060627	Regulation of vesicle-mediated transport	6 of 551	1.00	1.92e-09	
GO:0005200	Structural constituent of cytoskeleton	4 of 107	1.51	0.0206	

Fig. 1. (**A**) Heatmap with hierarchical clustering of the transcriptomic analysis data. The relative expression level of each gene is indicated by the color bar: green, lowest; red, highest. (**B**) STRING protein-protein interaction network of the 23 differentially expressed genes associated with DCM. Edges represent the protein-protein associations evidenced by curated databases (blue line), experimental determination (pink line), coexpression (black line) and protein homology (lavender line). Positive and negative correlations between mRNA expression in DCM patients are represented by green lines and red lines, respectively. Node colors represent different enriched GO terms with FDR < 0.05. CNT, control; DCM, dilated cardiomyopathy; FDR, false discovery rate.

			Function	r	p
Golgi membrane component	*GOLGA2*	*CDK5*	Vesicle-mediated transport	0.560	0.047
		RAB9A		0.731	0.005
		RAB9B		0.604	0.029
		KIF13A		0.594	0.032
		SORT1		0.816	0.001
		AP1M1		0.569	0.043
		TUBA4	Structural constituent of cytoskeleton	0.561	0.046
Vesicle-mediated transport	*RAB9A*	*RAB9B*	Vesicle-mediated transport	0.775	0.002
		RAB29		0.576	0.039
		KIF13A		0.625	0.022
		VTI1A		0.607	0.028
		CASP2	Caspase	− 0.694	0.008
	RAB9B	*RAB29*	Vesicle-mediated transport	0.641	0.018
		KIF13A		0.609	0.027
		CLIP3	Regulation of vesicle-mediated transport	− 0.655	0.015
		CASP2	Caspase	− 0.729	0.005
	RAB29	*CLIP3*	Regulation of vesicle-mediated transport	− 0.664	0.013
		CASP2	Caspase	− 0.632	0.020
	CDK5	*ATP2C1*	Regulation of vesicle-mediated transport	− 0.733	0.004
	AP1S2	*TRAPPC2*	Vesicle-mediated transport	0.753	0.005
		CASP2	Caspase	− 0.554	0.049
	SORT1	*KIF13A*	Vesicle-mediated transport	0.654	0.015
	AP1M1	*TUBA1A*	Structural constituent of cytoskeleton	0.645	0.017
		TUBA4A		0.699	0.008
Structural constituent of cytoskeleton	*ACTA1*	*TUBA3E*	Structural constituent of cytoskeleton	− 0.605	0.028
		TUBA4A		− 0.698	0.008
Caspase	*CASP2*	*TMF1*	Golgi membrane component	− 0.707	0.007
		CLIP3	Regulation of vesicle-mediated transport	0.633	0.020

Table 2. Relationships between differentially expressed genes in patients with dilated cardiomyopathy.

(FC = − 1.50, $p < 0.01$), and two SNAREs, *VAMP4* (FC = − 1.27, $p < 0.05$) and *VTI1A* (FC = − 1.57, $p < 0.01$) were downregulated (Fig. 3B). Transport in both directions is dependent on the luminal [Ca^{2+}] in the GA. Therefore, we examined genes involved in calcium homeostasis and we detected the upregulation of a calcium-transporting ATPase, *ATP2C1* (FC = 1.33, $p < 0.001$) (Fig. 3C).

GA fragmentation in DOX-induced DCM in cells

To visualize possible GA fragmentation in DCM, we used AC16 human cardiomyocytes treated with DOX as an in vitro DCM model because it is widely known that this drug induces cardiomyopathy. We stained the cells with an antibody against GM130 to identify the GA structure via fluorescence microscopy in three independent experiments. Notably, DOX treatment caused morphological changes in these organelles (Fig. 4A). To quantify this altered phenotype, we measured the number of Golgi fragments per cell, and we detected a significant increase in DOX-treated cells compared with CNT cells (FC = 1.54, $p < 0.05$). We observed that 70.2% of the cells treated with DOX presented GA fragmentation, whereas only 34.1% of the CNT cells did (FC = 2.06, $p < 0.001$). We previously showed that cardiomyocytes from patients with DCM presented 60% larger nuclei than did those from patients in the CNT group[24]. Therefore, we measured the nuclear area of cells showing a similar increase to that previously observed in patients in the nuclear area of DOX-treated cardiomyocytes compared to untreated cells (FC = 1.65, $p < 0.05$) (Fig. 4B).

In addition, we analyzed the expression levels of the *GOLGA2* gene in DOX-treated cells since this gene is closely related to Golgi fragmentation. We observed decreased mRNA expression of *GOLGA2* in cells treated with DOX (FC = − 1,45, $p < 0.001$), as occurred in the tissues of patients with DCM (Fig. 4C). In DOX-treated cells, we also detected upregulation of *NPPB* (FC = 43.46, $p < 0.001$), the gene encoding BNP, which also occurred in tissues from patients with DCM (Fig. 4C). Interestingly, the expression of the genes was negatively correlated ($r = -0.906$, $p < 0.001$). Since these results corroborate those observed in patients with DCM, we also analyzed BNP levels in cell culture supernatant samples and observed higher levels in the supernatants of DOX-treated cultures than in those from untreated cells (FC = 2.07, $p < 0.001$).

Discussion

Golgi fragmentation is a nonspecific ultrastructural finding and can be the consequence of numerous molecular events. In fact, it occurs during many physiological processes, such as mitosis and apoptosis[7], in addition to

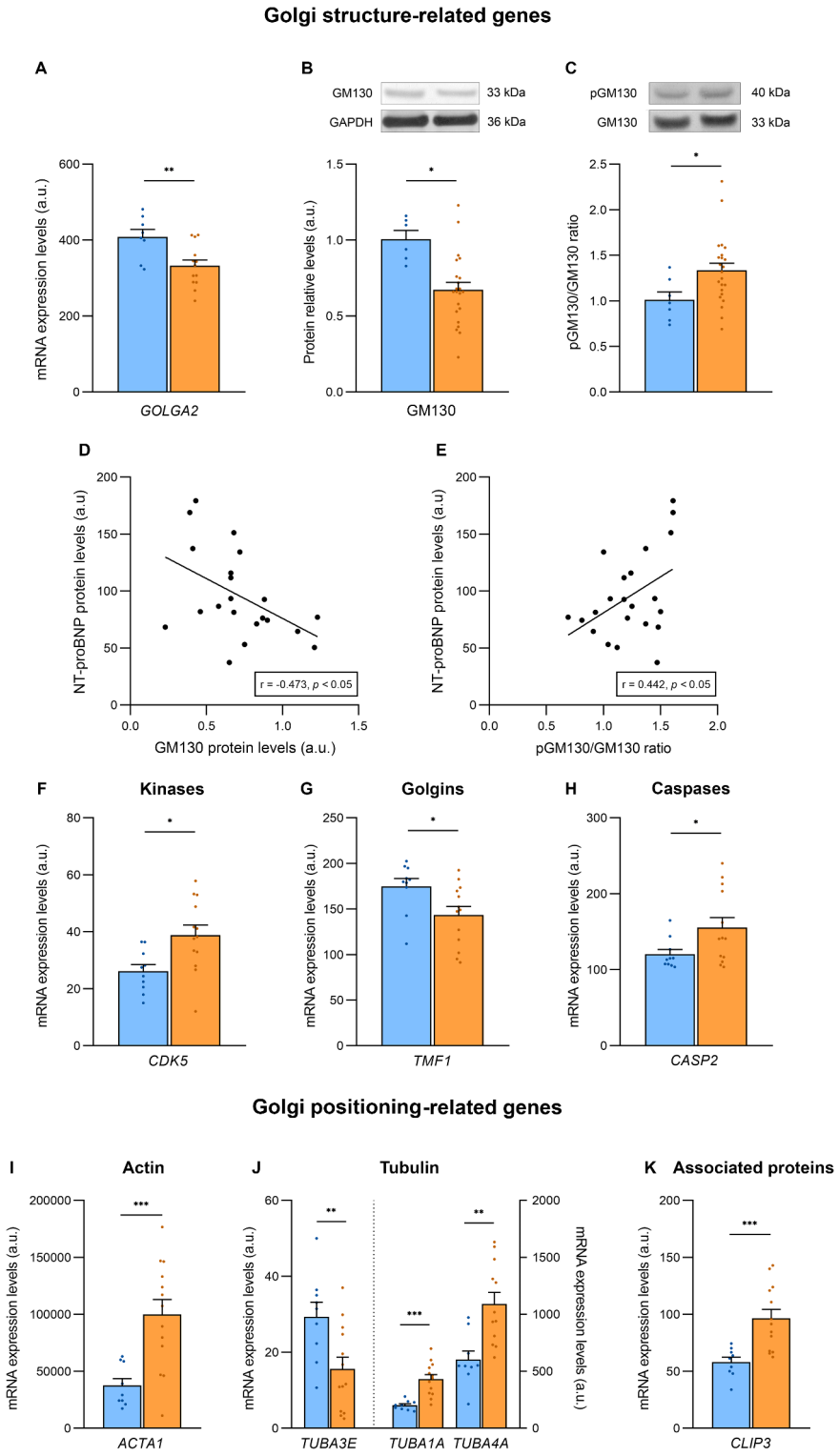

Fig. 2. Alterations in molecules related to the Golgi structure and positioning in dilated cardiomyopathy. (**A**) Relative mRNA expression levels of *GOLGA2*. (**B**) Relative protein expression levels of GM130. (**C**) p-GM130 vs. total GM130 protein ratio. (**D**, **E**) Correlations between GM130 levels and the ratio of GM130 phosphorylation to NT-proBNP levels in tissue. (**F**) Relative mRNA expression levels of the kinase *CDK5*. (**G**) Relative mRNA expression levels of golgin *TMF1*. (**H**) Relative mRNA expression levels of the caspase *CASP2*. (**I**) Relative mRNA expression levels of the actin subunit *ACTA1*. (**J**) Relative mRNA expression levels of tubulin genes. (**K**) Relative mRNA expression levels of *CLIP3*. Data are presented as the means ± SEMs. a.u., arbitrary units. Controls (blue), dilated cardiomyopathy (orange). $^{*}p < 0.05$, $^{**}p < 0.01$, $^{***}p < 0.001$. Original uncropped blots are presented in Supplementary Fig. S1 in the Supplementary Information file.

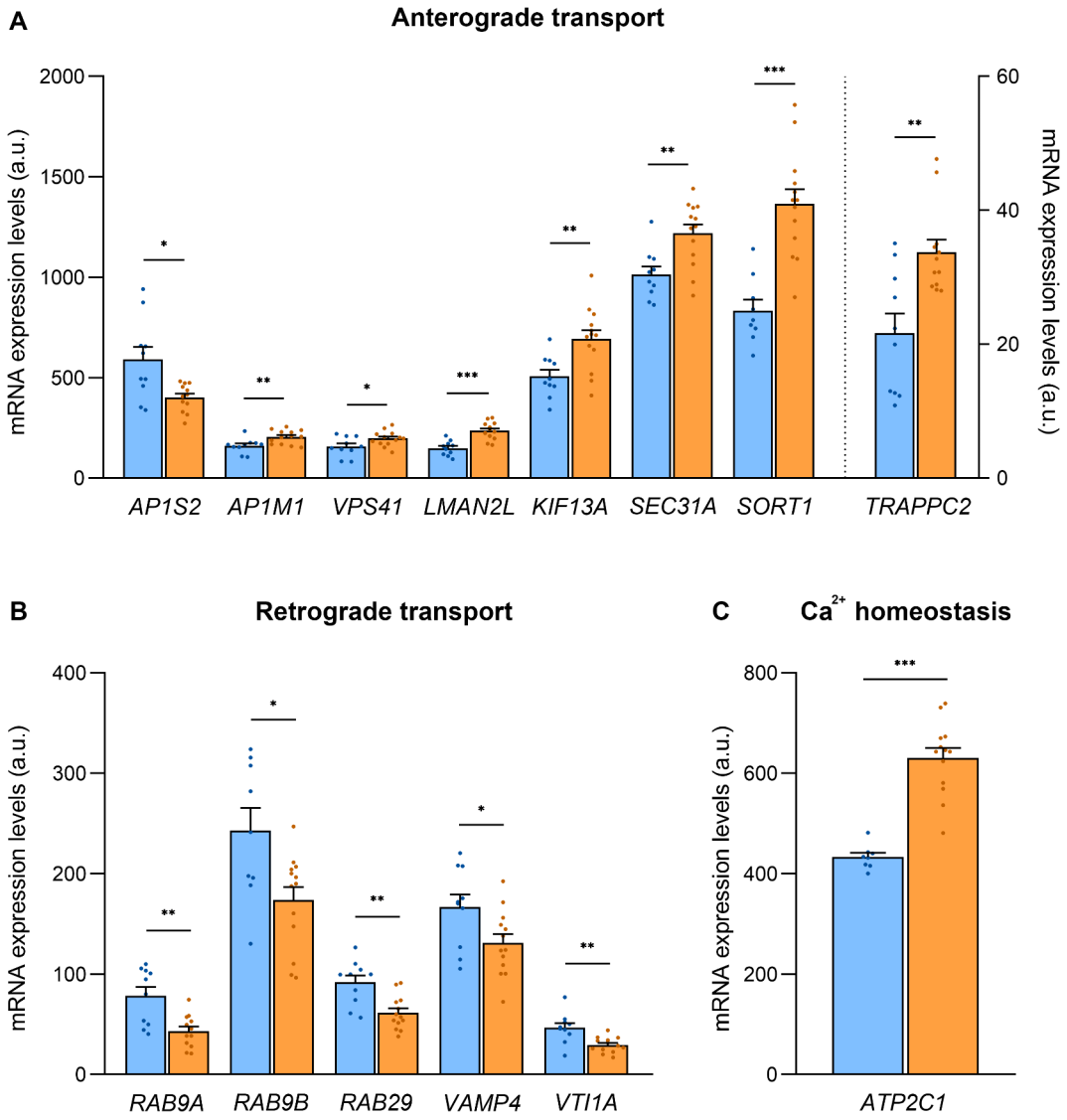

Fig. 3. Alterations in molecules involved in vesicle transport in dilated cardiomyopathy. (**A**) Relative mRNA expression levels of genes with a role in anterograde transport. (**B**) Relative mRNA expression levels of genes with a role in retrograde transport. (**C**) Relative mRNA expression levels of *ATP2C1*. Data are presented as the means ± SEMs. a.u., arbitrary units. Controls (blue), dilated cardiomyopathy (orange). $^{*}p < 0.05$, $^{**}p < 0.01$, $^{***}p < 0.001$.

other pathological molecular events, and has been observed in diseases such as Alzheimer's disease[8] and cancer[9]. Although the Golgi complex is a highly dynamic cellular organelle, it maintains a distinct morphology with high stability. However, physiological conditions are known to change the shape of the Golgi, including disassembly during mitosis, which causes Golgi fragmentation into mini stacks, and irreversible fragmentation during apoptosis[25]. In addition, there is increasing evidence that Golgi fragmentation is associated with pathological conditions, emerging as an early histological sign of cellular damage prior to apoptosis in multiple disorders, including neurodegenerative diseases[26].

In our previous study, we observed a greater density of GA vesicles in patients with DCM than in CNT individuals, and these vesicles were smaller and more ellipsoidal. We attributed the increase in GA vesicles and their morphological changes to a greater demand for NPs in patients with HF, with the purpose of regulating plasma volume and pressure homeostasis[12]. Several studies have reported an increased rate of protein transport when the GA is partially unstacked, since the fragmented GA has a larger area available for vesicle formation than the compact GA does[27]. The increased rate of transport may be a compensatory reaction in situations where a greater quantity of protein is needed[8,28]. This could explain our previous observation, therefore, we studied the state of the GA in patients with DCM, analyzing the expression of various genes involved in GA structure and positioning and vesicle transport, whose alteration could lead to GA fragmentation (Fig. 5).

GOLGA2 encodes GM130, which plays an important role in maintaining the GA structure and tethering transport vesicles from the ER to the Golgi membrane. Numerous studies have shown that loss of GM130 disrupts

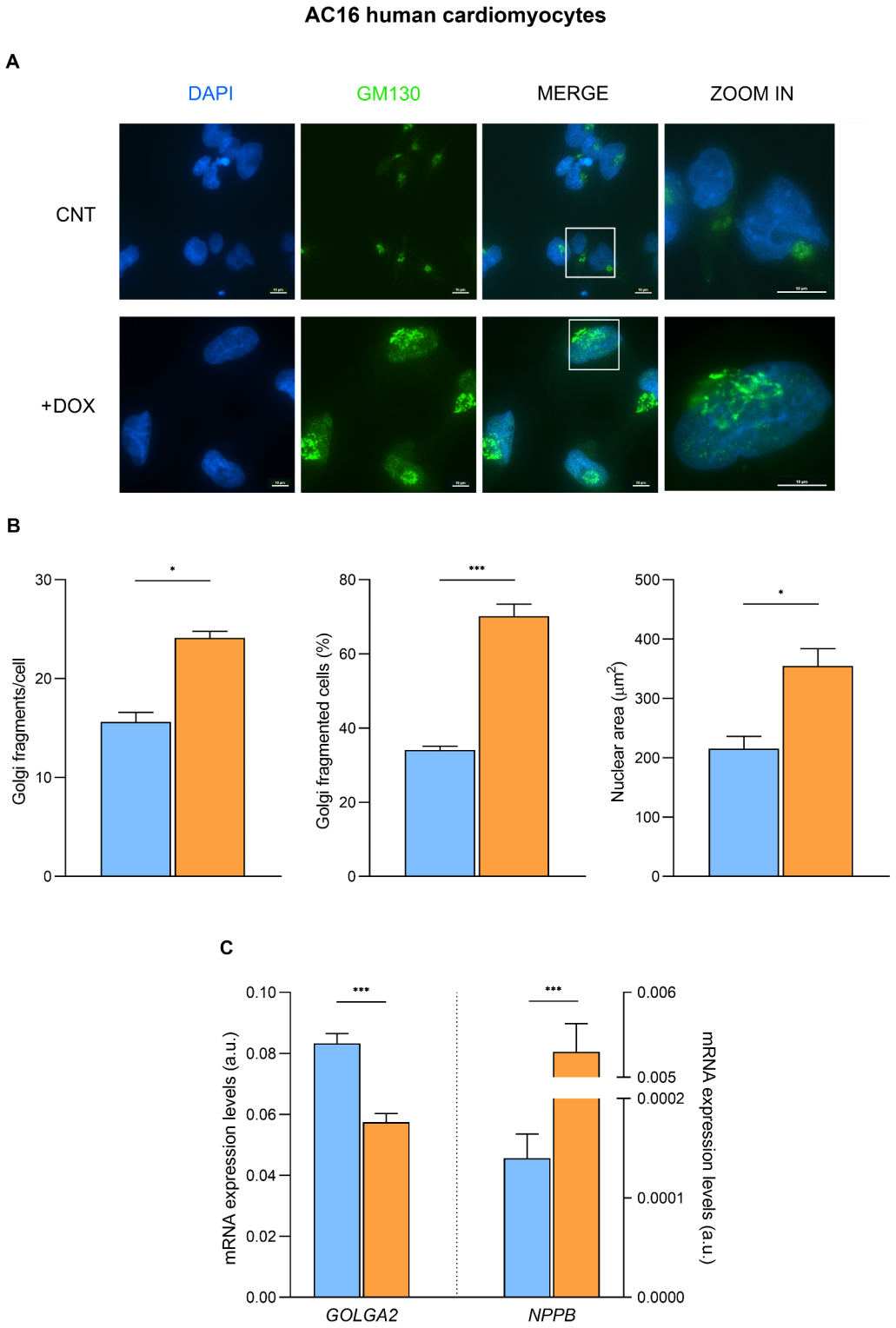

Fig. 4. Golgi fragmentation in DOX-induced dilated cardiomyopathy in AC16 cells. (**A**) Representative images of nontreated (CNT) or DOX-treated (DOX) cardiomyocytes immunostained for the Golgi marker GM130 (green) and the nuclear marker DAPI (blue). Scale bars, 10 μm. Boxed regions are enlarged and shown on the right. (**B**) Quantification of Golgi fragments, the percentage of cells with fragmented Golgi (> 15 Golgi fragments < 1 μm^2) and the nucleus area. (**C**) Relative mRNA expression levels of *GOLGA2* and *NPPB*. Data are presented as the means ± SEMS from three independent experiments. Control cells (blue), DOX-treated cells (orange). $^*p < 0.05$, $^{***}p < 0.001$.

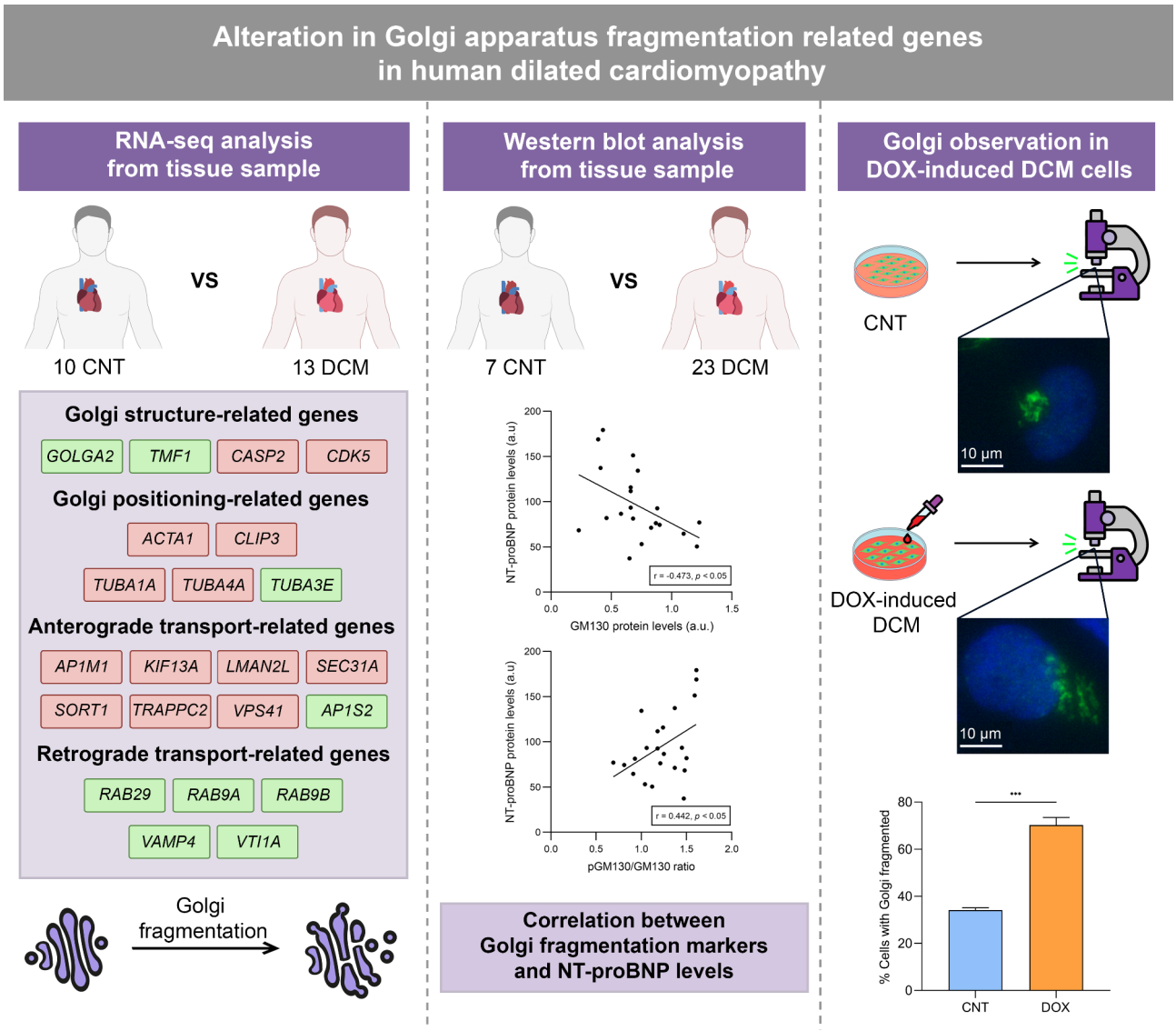

Fig. 5. Alterations in Golgi-related genes suggest disruption of the Golgi structure, which we observed in an in vitro DCM model, related to natriuretic peptide levels. Upregulated genes, red; downregulated genes, green. CNT, control; DCM, dilated cardiomyopathy; NT-proBNP, N-terminal pro b-type natriuretic peptide; DOX, doxorubicin.

the structure and alters the position of the GA[10]. In patients with DCM, we found that GM130 was downregulated at the mRNA and protein levels. Moreover, its phosphorylation at Ser25 leads to GA fragmentation; due to inhibited vesicle fusion with continuous budding[11,29]. We also observed an increase in the p-GM130/GM130 ratio in patients with DCM. Our results report for the first time that GM130 is altered in ventricular tissue from patients with DCM and suggest GA fragmentation. In accordance with the increased ratio of GM130 phosphorylation, we detected an increase in the level of *CDK5*, a kinase responsible for this modification[11].

Furthermore, we found a correlation between the GM130 level, as well as its phosphorylation ratio, with the NT-proBNP level in cardiac tissue. Although this NP is regarded as biologically inactive, it is widely used as a diagnostic and prognostic biomarker in HF[13]. Its production and release by the heart increase in response to wall stress due to volume or pressure overload. Our data open new avenues for further study to confirm that GA fragmentation could be related to the increased secretion of NP in DCM, in the same way that a compensatory reaction has been described in situations in which a higher amount of proteins is needed[8,28]. GM130 is not the only golgin we found to be altered; *TMF1* was also downregulated, which could contribute to Golgi disruption, since low levels of this protein promote Golgi dispersion[30]. The structure and positioning of the GA also depend on the cytoskeleton. Compared with those in CNT individuals, genes encoding actin (*ACTA1*) and tubulin subunits (*TUBA1A*, *TUBA3E* and *TUBA4A*) in patients with DCM were altered. Although it seems that GA fragmentation occurs independently of changes in the cytoskeleton during early apoptosis[31] and Parkinson's disease[32], disruption of microtubules and perturbation of the union between actin and GA induce changes in Golgi structure and vesicle transport[33]. Therefore, more studies are needed to determine whether this alteration

in cytoskeleton subunits plays a role in GA fragmentation in DCM. We also observed that the expression of *CLIP3*, a protein localized in the trans-Golgi network (TGN) that has a microtubule-binding domain was upregulated. *CLIP3* upregulation perturbs the TGN compartment and retrograde transport[34].

Moreover, GA structure depends partly on vesicles entering and leaving the organelle, i.e., the balance between anterograde and retrograde transport[7]. Thus, a dysregulation of transport machinery molecules may be responsible for GA disruption[6]. In this sense, in patients with DCM compared with CNT individuals, most of the altered genes related to anterograde transport were upregulated, whereas all altered genes involved in retrograde transport were downregulated. These findings suggest continued budding of transport vesicles, whereas fusion to the Golgi membrane is reduced, which could lead to vesiculation of the GA and, ultimately, its fragmentation. This finding is consistent with the greater number of GA vesicles that observed in our previous work[12] and in other studies, which proved that some of these described alterations cause GA fragmentation, such as *RAB29*[35], *VAMP4* and *VTI1A*[36]. In addition, we found an upregulation of *ATP2C1* which encodes SPCA1 that regulates Ca^{2+} homeostasis and thus vesicle transport. It has been reported that its upregulation induces GA fragmentation[26].

Furthermore, we visualized the expected GA fragmentation in AC16 human cardiomyocytes treated with DOX. Treatment with DOX led to DCM in patients[37], and is used for in vitro[37] and in vivo[38] DCM models. In a mouse model, this drug increases ventricular diameters and causes similar clinical symptoms to DCM[38]. DOX treatment of cardiomyocytes is used to simulate DCM in vitro to study the underlying molecular mechanisms[37]. We observed larger nuclei in DOX-treated cells than in untreated cells, which is in accordance with our previous study that revealed an increase in nucleus size in patients with DCM compared with that in CNT individuals[24]. This similar observation supports the use of DOX treatment in cardiomyocytes to induce the DCM phenotype. Fluorescence imaging analysis revealed an increase in the number of GA fragments per cell as well as in the percentage of cells with GA fragmentation in DOX-induced DCM cardiomyocytes. This observation is in accordance with the alteration in GA organization suggested by our transcriptomic study. Previously, Muhammad et al. reported GA dispersion in the fibroblast of patients with DCM; however, to our knowledge, this is the first time that GA fragmentation has been described in the cardiac tissue of patients with DCM. The loss of *GOLGA2* is widely shown to be a marker of GA fragmentation[10]. In the same way that we observed in patients with DCM, we observed this downregulation in DOX-induced DCM AC16 cells, revealing the key role of this gene in maintaining GA structure. Our hypothesis relates GA disruption to increased secretion of demanded NPs, as we previously observed in patients with DCM[12]. In accordance with these findings, *NPPB* was upregulated in DOX-treated AC16 cells, as previously observed in other DOX-treated cell types[39], and furthermore was negatively correlated with *GOLGA2*. Moreover, BNP levels in the supernatants of DOX-treated cardiomyocytes were greater than those in the supernatants of untreated cardiomyocytes. These observations suggest that GA fragmentation is related to increased NP secretion.

A limitation of this study is the use of cardiac samples from patients with end-stage HF, who exhibit high variability in disease etiology and treatment. The treatments received by the patients may have affected the results obtained. Nevertheless, this was carried out with an etiologically homogeneous population; patients with DCM who did not report any family history of the disease were chosen, and all individuals had been receiving medical treatment according to the guidelines of the European Society of Cardiology[13].

In summary, this study revealed alterations in several Golgi-related molecules, including golgins, cytoskeleton subunits and transport machinery proteins in patients with DCM. Many of them have been described as causes of GA fragmentation, especially GM130. Our results suggest disruption of the Golgi structure, which we observed in DOX-induced DCM cardiomyocytes.Although more work is needed to fully understand the role of GA fragmentation in this disease, it could provide new insights into cardiac dysfunction in DCM patients.

Data availability

The data presented in this manuscript have been deposited in the NCBI's Gene Expression Omnibus (GEO) database and are accessible through the GEO series accession number GSE55296 (http://www.ncbi.nlm.nih.gov/geo/query/acc.cgi? acc=GSE55296). All other supporting data from this study are available from the corresponding author upon reasonable request.

Received: 1 August 2024; Accepted: 3 March 2025
Published online: 05 March 2025

References

1. Finocchiaro, G. et al. The electrocardiogram in the diagnosis and management of patients with dilated cardiomyopathy. *Eur. J. Heart Fail.* **22**, 1097–1107 (2020).
2. Schultheiss, H. P. et al. Dilated cardiomyopathy. *Nat. Rev. Dis. Primers*. **5**, 32 (2019).
3. Shankar, T. S. et al. Cardiac-specific deletion of voltage dependent anion channel 2 leads to dilated cardiomyopathy by altering calcium homeostasis. *Nat. Commun.* **12**, 4583 (2021).
4. Ramaccini, D. et al. Mitochondrial function and dysfunction in dilated cardiomyopathy. *Front. Cell. Dev. Biol.* **8**, 624216 (2021).
5. Ortega, A. et al. Endoplasmic reticulum stress induces different molecular structural alterations in human dilated and ischemic cardiomyopathy. *PLoS One*. **9**, e107635 (2014).
6. Martínez-Menárguez, J. Á., Tomás, M. & Martínez-Martínez, N. Martínez-Alonso, E. Golgi fragmentation in neurodegenerative diseases: Is there a common cause?? *Cells* **8**, 748 (2019).
7. Makhoul, C., Gosavi, P. & Gleeson, P. A. The golgi architecture and cell sensing. *Biochem. Soc. Trans.* **46**, 1063–1072 (2018).
8. Joshi, G., Chi, Y., Huang, Z. & Wang, Y. Aβ-induced golgi fragmentation in Alzheimer's disease enhances Aβ production. *Proc. Natl. Acad. Sci. U S A*. **111**, E1230–E1239 (2014).
9. Zhang, X. Alterations of golgi structural proteins and glycosylation defects in Cancer. *Front. Cell. Dev. Biol.* **9**, 665289 (2021).
10. Liu, C. et al. Loss of the golgin GM130 causes golgi disruption, purkinje neuron loss, and ataxia in mice. *Proc. Natl. Acad. Sci. U S A*. **114**, 346–351 (2017).

11. Sun, K. H. et al. Novel genetic tools reveal Cdk5's major role in golgi fragmentation in Alzheimer's disease. *Mol. Biol. Cell.* **19**, 3052–3069 (2008).
12. Tarazón, E. et al. Changes in human golgi apparatus reflect new left ventricular dimensions and function in dilated cardiomyopathy patients. *Eur. J. Heart Fail.* **19**, 280–282 (2017).
13. McDonagh, T. A. et al. 2021 ESC guidelines for the diagnosis and treatment of acute and chronic heart failure. *Eur. Heart J.* **42**, 3599–3726 (2021).
14. Macrae, D. J. The Council for international organizations and medical sciences (CIOMS) guidelines on ethics of clinical trials. *Proc. Am. Thorac. Soc.* **4**, 176–179 (2007).
15. Roselló-Lletí, E. et al. Human ischemic cardiomyopathy shows cardiac Nos1 translocation and its increased levels are related to left ventricular performance. *Sci. Rep.* **6**, 24060 (2016).
16. Winters, A. L. & Minchin, F. R. Modification of the Lowry assay to measure proteins and phenols in covalently bound complexes. *Anal. Biochem.* **346**, 43–48 (2005).
17. Nozawa, T. et al. Intracellular group A Streptococcus induces golgi fragmentation to impair host defenses through streptolysin O and NAD-Glycohydrolase. *mBio* **12**, e01974–e01920 (2021).
18. Livak, K. J. & Schmittgen, T. D. Analysis of relative gene expression data using Real-Time quantitative PCR and the 2 – ΔΔCT method. *Methods* **25**, 402–408 (2001).
19. Love, M. I., Huber, W. & Anders, S. Moderated Estimation of fold change and dispersion for RNA-seq data with DESeq2. *Genome Biol.* **15**, 550 (2014).
20. Benjamini, Y. & Hochberg, Y. Controlling the false discovery rate: A practical and powerful approach to multiple testing. *J. R Stat. Soc. Ser. B Stat. Methodol.* **57**, 289–300 (1995).
21. Trapnell, C. et al. Transcript assembly and quantification by RNA-Seq reveals unannotated transcripts and isoform switching during cell differentiation. *Nat. Biotechnol.* **28**, 511–515 (2010).
22. Anders, S. & Huber, W. Differential expression analysis for sequence count data. *Genome Biol.* **11**, R106 (2010).
23. Robinson, M. D., McCarthy, D. J. & Smyth, G. K. EdgeR: A bioconductor package for differential expression analysis of digital gene expression data. *Bioinformatics* **26**, 139–140 (2010).
24. Cortés, R. et al. Nuclear changes and p62 expression in ischemic and dilated cardiomyopathy. *Rev. Esp. Cardiol.* **60**, 1319–1323 (2007).
25. Thayer, D. A., Jan, Y. N. & Jan, L. Y. Increased neuronal activity fragments the Golgi complex. *Proc. Natl. Acad. Sci.* **110**, 1482–1487 (2013).
26. Bhojwani-Cabrera, A. M. et al. Upregulation of the secretory pathway Ca2+/Mn2+-ATPase isoform 1 in LPS-stimulated microglia and its involvement in Mn2+-induced golgi fragmentation. *Glia* **72**, 1201–1214 (2024).
27. Read, C. B. et al. Ceramide-1-phosphate is a regulator of golgi structure and is co-opted by the obligate intracellular bacterial pathogen *Anaplasma phagocytophilum*. *mBio* **15**, e0029924 (2024).
28. Wang, Y., Wei, J. H., Bisel, B., Tang, D. & Seemann, J. Golgi cisternal unstacking stimulates COPI vesicle budding and protein transport. *PLoS One*. **3**, e1647 (2008).
29. Lowe, M., Gonatas, N. K. & Warren, G. The mitotic phosphorylation cycle of the Cis-Golgi matrix protein GM130. *J. Cell. Biol.* **149**, 341–356 (2000).
30. Fridmann-Sirkis, Y., Siniossoglou, S. & Pelham, H. R. TMF is a golgin that binds Rab6 and influences golgi morphology. *BMC Cell. Biol.* **5**, 18 (2004).
31. Mukherjee, S., Chiu, R., Leung, S. & Shields, D. Fragmentation of the golgi apparatus: An early apoptotic event independent of the cytoskeleton. *Traffic* **8**, 369–378 (2007).
32. Rendón, W. O., Martínez-Alonso, E., Tomás, M., Martínez-Martínez, N. & Martínez-Menárguez, J. A. Golgi fragmentation is Rab and SNARE dependent in cellular models of Parkinson's disease. *Histochem. Cell. Biol.* **139**, 671–684 (2013).
33. Buschman, M. D., Xing, M. & Field, S. J. The GOLPH3 pathway regulates golgi shape and function and is activated by DNA damage. *Front. Neurosci.* **9**, 362 (2015).
34. Perez, F. et al. CLIPR-59, a new trans-Golgi/TGN cytoplasmic linker protein belonging to the CLIP-170 family. *J. Cell. Biol.* **156**, 631–642 (2002).
35. Wang, S. et al. A role of Rab29 in the integrity of the trans-Golgi network and retrograde trafficking of mannose-6-phosphate receptor. *PLoS One*. **9**, e96242 (2014).
36. Shitara, A. et al. VAMP4 is required to maintain the ribbon structure of the golgi apparatus. *Mol. Cell. Biochem.* **380**, 11–21 (2013).
37. Zhang, S. et al. Doxorubicin downregulates autophagy to promote apoptosis-induced dilated cardiomyopathy via regulating the AMPK/mTOR pathway. *Biomed. Pharmacother.* **162**, 114691 (2023).
38. Leontyev, S. et al. Transplantation of engineered heart tissue as a biological cardiac assist device for treatment of dilated cardiomyopathy. *Eur. J. Heart Fail.* **15**, 23–35 (2013).
39. Hwang, S. et al. Exogenous 8-hydroxydeoxyguanosine attenuates doxorubicin-induced cardiotoxicity by decreasing pyroptosis in H9c2 cardiomyocytes. *BMC Mol. Cell. Biol.* **23**, 55 (2022).

Acknowledgements

The authors are grateful to Manuel Vázquez-Carrera from School of Pharmacy and Food Sciences of University of Barcelona for their technical support.

Author contributions

MP, ET, ERL designed and supervised the study, IGT, IGE conducting experiments, LPC, MDA acquiring and analysing data, MP, ET, ERL, LPC contributed to data interpretation and/or discussion; IGT, IGE writing the manuscript. All authors reviewed the manuscript.

Funding

This work was supported by the National Institute of Health "Fondo de Investigaciones Sanitarias del Instituto de Salud Carlos III" (Projects: PI20/01469, PI20/00071) co-funded by European Union; Miguel Servet contract: (CP21/00041) co-funded by European Union; (contracts FI21/00186 and FI21/00034); "Consorcio Centro de Investigación Biomédica en Red" (CIBERCV, under Grant CB16/11/00261); Ministry of Science and Innovation (MCIN, https://doi.org/10.13039/501100011033) and State Investigation Agency (AEI) (Project CNS2022-13 5769) co-funded by European Union "Next Generation EU" and the European Recovery, Transformation and Resilience Plan (PRTR); Conselleria de educación, universidades y empleo (Project CIAICO/2022/246, contract CIACIF/2022/429).

Declarations

Competing interests
The authors declare no competing interests.

Additional information
Supplementary Information The online version contains supplementary material available at https://doi.org/10.1038/s41598-025-92758-3.

Correspondence and requests for materials should be addressed to E.T. or E.R.-L.

Reprints and permissions information is available at www.nature.com/reprints.

Publisher's note Springer Nature remains neutral with regard to jurisdictional claims in published maps and institutional affiliations.